ERF European Rotorcraft Forum

EVALUATION OF FUNCTIONALITY AND MASS OF TWO IVT-DRIVES IN HELICOPTER-COMPOUND SPLIT DRIVETRAINS

Lorenz Braumann, lorenz.braumann@zoerkler.at, Zoerkler Gears GmbH & Co KG (Austria)
Hanns Amri, hanns.amri@zoerkler.at, Zoerkler Gears GmbH & Co KG (Austria)
Matthias Zoeggeler, matthias.zoeggeler@zoerkler.at, Zoerkler Gears GmbH & Co KG (Austria)

July 12, 2021

Abstract

The research described in this paper is part of the international research project VARI-SPEED. The aim of this project is to enable main rotor speed variation of rotorcraft in order to reduce the required propulsion power, which enables modern and ecologically efficient aviation. Application of an infinitely variable transmission, capable of speed ratios from $-\infty$ to 0, inside the helicopters compound-split module allows for seamless change of rotor speed within a ratio spread of 1.5. This study investigates whether two continuously variable transmission concepts based on the principle of the freewheel and the NuVinci traction drive satisfy the boundary conditions with regard to speed ratio range, mass and power transmission capability for a helicopter of the CS29 class. The general functionality is described for both transmission concepts and kinematic as well as force models are given in order to allow for a rough design, which acts as a base for the mass calculation. Validation for the freewheel gearbox is performed via multi-body dynamics simulation in SIMPACK and gear design in KISSsoft. The design of the traction drive is accomplished by implementation of a parametric model in MATLAB and fully automatic optimization by genetic algorithm. Although the freewheel gearbox allows a transmission ratio of $-\infty$ to -1, the necessary speed ratio of $-\infty$ to 0 could not be achieved. The traction drive concept, although capable of the required transmission ratio, is impaired significantly by recirculating power and much greater mass than the reference hydraulic variator unit utilized in previous publications. These findings are important for choosing the best infinitely variable transmission for application in the compound split drivetrain investigated in VARI-SPEED.

1 INTRODUCTION

The development of new rotorcraft configurations like compound rotorcraft or tiltrotor rotorcraft enables rotorcraft to fly fast forward and to have excellent hover and vertical take-off and landing (VTOL) capabilities. This development is pushed forward by two major research programs, the USA "*Future Vertical Lift*" (FVL) [1] program and the European Union's "*Clean Sky 2 - Fast Rotorcraft*" program [2]. Besides the requirements on the flight envelope also the efficiency of the rotorcraft is playing a major role. Rotor speed variation could be a key technology to increase rotorcraft efficiency.

It was shown by the Airbus Helicopters high-speed demonstrator X^3 that rotor speed variation could have benefits: The X^3 is a compound rotorcraft with one single main rotor and two tractor propellers mounted on small wings on each side of the rotorcraft. The main rotor speed is reduced in fast forward flight by variability of the turboshaft engine. The required additional thrust was provided by the two tractor propellers and the wings provided additional lift. This setting enabled the X^3 demonstrator to achieve an unofficial level-flight speed record of $255kt$ ($472km/h$) in June 2013 [3].

Variation of rotor speed by variability of the turboshaft engine does not only have advantages, as G.A. Miste concluded in his doctoral thesis [4]. He presented an optimization of variable turbo shaft engine performance with main rotor interaction of the T-700 UH-60A engine and the UH-60A main rotor. He found out that the RPM variation has a significant impact on the specific fuel consumption (SFC) of the turboshaft engine. The main rotor RPM variation performed by the turboshaft RPM variation is less efficient than an independent optimization of the main rotor RPM and turboshaft engine RPM.

The National Aeronautic and Space Administration (NASA) was looking for alternatives to vary the rotor speed in their *Heavy Lift Rotorcraft System Investigation* [5]. Three different passenger transport rotorcraft configurations were investigated. The so called *Large Civil Tiltrotor Concept*, a tiltrotor rotorcraft, was identified with the highest potential. It requires a rotor speed variation range of about 50% of the nominal RPM to be economically competitive [6]. To enable rotor speed variation three different concepts for

Presented at 47th European Rotorcraft Forum, United Kingdom, 7-9th September, 2021

transmission ratio variation with the drivetrain systems were developed: An inline two speed planetary gear, an offset compound gear and a planetary differential drive [7].

An investigation of possible benefits of variable rotor speed was performed by H. Amri et. al. [8]. In a CAMRAD II simulation model of a CS-27 class helicopter a reduction of required power of 23% could be achieved and different technology categories to enable rotor speed variation as well as the major risks and problems were identified.

Further investigations regarding the efficiency increase were performed by W. Garre et. al. [9]. Garre analyzed the possible efficiency increase and enhancement of the flight envelope with rotor speed variation for five different rotorcraft configurations: a single main rotor, a coaxial rotor, a coaxial compound, a tandem and a tiltrotor configuration. It was shown that a rotor speed variation of up to 50% of the nominal RPM is useful for all rotorcraft configurations, but there are always some flight states where rotor speed variation is not suitable. This is at the original design region of the rotorcraft, where the reference rotor speed is equal to the optimum rotor speed.

Based on the outcome of the investigation W. Garre et. al. [10] analyzed the rotor speed variation performance in the context of missions for five different rotorcraft configurations. They made a comparison between a single rotor speed, a two speed and a continuously variable transmission (CVT) variant within the missions. CVT systems showed the best benefits for utility rotorcraft. For fast rotorcraft, like compound or tiltrotor rotorcraft, the two speed transmission gains almost the same benefits as the CVT. For all configurations an efficiency increase could be identified. The drivetrain itself was not taken into account.

An investigation of the kinematic behavior and the mass of different compound split configurations was performed by H. Amri et. al. [11]. The investigation showed that the power flow in the variator path is the same for all configurations and it depends only on the spread (ratio of highest output speed to lowest output speed). The mass of the compound split configurations is different and depends on the basic transmission ratio (ratio of the input speed to the highest output speed) and the spread. They concluded that a compound split variation is most suitable when it has the lowest mass at a high basic transmission ratio in a given range of spread.

H. Amri et. al. [12] developed a mass estimation model for the Sikorsky UH-60A drivetrain including a compound split. Hydraulic, electric and mechanic variator technologies were investigated regarding their mass, torque and RPM properties. An optimization model was set up to find the best variator technology for the mass optimized drivetrain. While at the moment the design is too heavy to gain benefits in efficiency, the electric variator technology seems to have the highest potential to enable an efficient variable rotor speed technology.

H. DeSmidt et al. investigated the dynamics and developed a thermal model for an Offset Compound Gear Transmission for dual-speed rotorcraft applications [13]. The focus of their work is on the thermal behaviour of the clutch. They concluded that the peak temperature and the temperature rise of the wet clutch is lower than those of the dry clutch. The peak temperature and the temperature rise of the wet clutch is proportional to the clutch oil flow rate.

One of open questions in this research is how the speed variation can be performed in the compound split module and if there is a possibility to solve the transmission variation by mechanical means. Therefore, this publication should:

- investigate the possible usage of two mechanical infinite variable transmission ratio systems.
- evaluate the additional mass of the systems.

2 THE FREEWHEEL IVT

2.1 Freewheel-IVT Model

2.1.1 Description freewheel gearbox

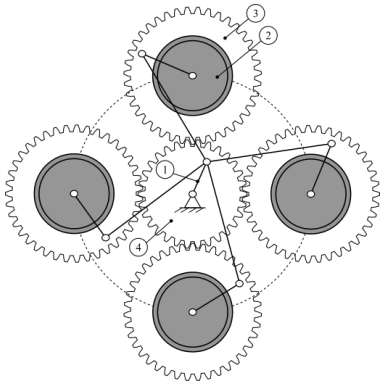

Figure 1. *Schematic illustration of the freewheel gearbox with its components: crank rockers (1), freewheels (2), planet wheel (3) and central wheel (4) [14]*

The function of the freewheel gearbox is achieved by the combination of several crank rockers (1), freewheels (2) and spur gears, see figure 1. The rocker is connected to the inner ring of the freewheel and the outer ring of the freewheel is connected to the planet wheel (3). The planet wheels are in common contact with the central wheel (4) and therefore have the same angular velocity. The output is represented by the central wheel.The change of the transmission ratio is achieved by varying the length of the crank [14]. The crank length is changed on the double eccentric principle [15]. When the crank length is zero, the input-shaft

Presented at 47th European Rotorcraft Forum, United Kingdom, 7-9th September, 2021

rotates and the output-shaft stands still and the transmission ratio is infinite. With the freewheel gearbox a transmission ratio of ∞ to about *one* can be achieved [14].

The crank rocker mechanism is set in motion by the crank located on the drive shaft and this drives the rockers and thus the freewheels. Depending on which rocker has the highest momentary speed, the freewheel locks and transmits power. The power transmission is always only performed by one planet wheel. By overlaying the oscillating swinging motion, a quasi-continuous output drive is achieved, see black dotted line in Figure 2 [14].

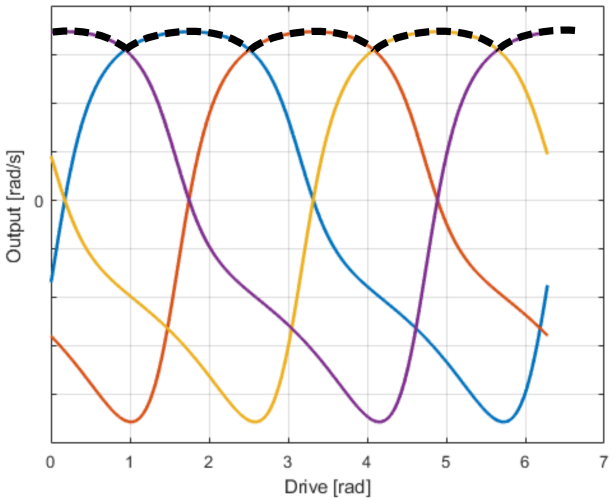

Figure 2. *Representation of the phase-shifted movements of the rocker arms [14]*

2.1.2 Kinematic Model

Due to the kinematic of the crank rockers, a speed fluctuation occurs in the freewheel gearbox. The speed fluctuation is the difference between the extreme values of the dotted line in Figure 2 [14]. It is necessary to choose the dimensions of the crank rocker mechanism to minimize the speed fluctuation.
The illustration in Figure 3 shows the mechanical model of a crank rocker with its links. With the one selected degree of freedom, the drive coordinate q, the movement of all links is defined. During a complete rotation of the crank, the rocker arm performs an oscillating movement, which is represented by the angle ψ_0.
With the Equation 1 the output angle γ of the rocker arm is defined. It can be seen that γ depends on all lengths of the links a, b, c and d as well as the drive coordinate q.

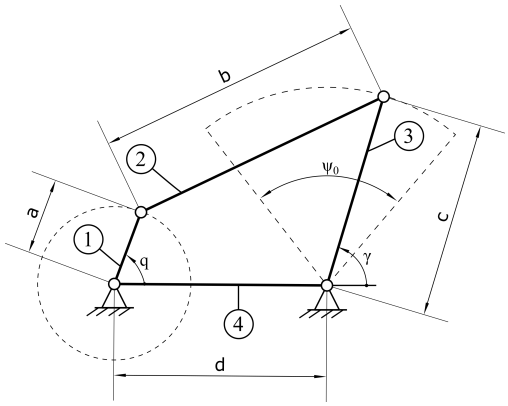

Figure 3. *Illustration of a crank rocker mechanism, with its components: crank (1), coupler (2), rocker arm (3) and frame (4) [16]*

$$\gamma = \pi - \arcsin\left(\frac{a * sin(q)}{\sqrt{a^2 + d^2 - 2 * a * d * \cos(q)}}\right) - \arccos\left(\frac{a^2 + d^2 - 2 * a * d * \cos(q) + c^2 - b^2}{2 * c * \sqrt{a^2 + d^2 - 2 * a * d * \cos(q)}}\right) \tag{1}$$

To determine the angular velocity $\dot{\gamma}$ of the rocker arm, γ is derived with respect to time. This is equal to the derivative of the degree of freedom q multiplied by the drive angular velocity $\dot{q}$, see Equation 2. The differentiation of the angle γ to q is done numerically in Matlab.

$$\dot{\gamma} = \frac{\mathrm{d}\gamma}{\mathrm{d}t} = \frac{\mathrm{d}\gamma}{\mathrm{d}q} \cdot \dot{q} = \gamma' \cdot \dot{q} \tag{2}$$

To minimize the speed fluctuation, many planet wheels should be arranged around the central wheel. Equation 3 shows that the possible number of planet gears depends only on the transmission ratio i_{St} between the central gear and one planet.

$$n = \frac{360°}{2 * \arcsin\left(\frac{1}{i_{St}+1}\right)} \tag{3}$$

If the lengths of the links as well as the number of planet wheels are known, the speed fluctuation can be determined.

2.1.3 Kinetic Model

A central role in the freewheel gearbox is played by the crank rocker, which serves to control the speed and transmit the movement [14]. The crank rocker must be dimensioned appropriately so that the joint forces that occur are low. This means that the components such as bearings can be dimensioned smaller.
According to the VDI-2130 guidelines[17], the centric

Presented at 47th European Rotorcraft Forum, United Kingdom, 7-9th September, 2021

crank rocker is used for the given application. The special feature of the centric crank rocker is that it is favourable in terms of transmission and acceleration. This means that for slow-running transmissions with high forces to be transmitted or for fast-running transmissions with high mass forces, this crank rocker type is preferred [17]. The centric crank rocker can be determined graphically with the design according to Hermann Alt, where the frame length d and the angles φ_0 and ψ_0 are required [16]. Figure 4 shows the design according to Hermann Alt [16] with a crank rocker in the outer dead-center positions, where crank and coupler are in the stretched positions. In this case, a frame length of $d = 200mm$ is used, since the compound split has an approximate diameter of $500mm$. The maximum oscillation angle of $\psi_0 = 120°$ is chosen to achieve the highest possible transmission ratio and for the centric crank rocker φ_0 is 180° [16]. A solution with $\beta = 15°$ and the corresponding link lengths of crank (a), coupler (b) and swing arm (c) are shown in Figure 4. The angle β indicates a possible solution of the centric crank rocker and can be varied from 0° to 30°.

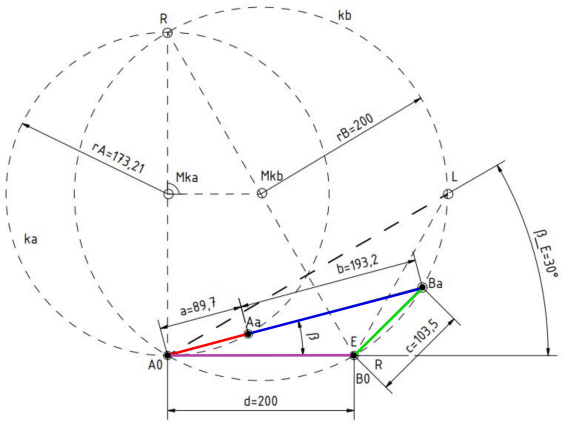

Figure 4. *Dead-Center constructions after Hermann Alt [16] for the centric crank rocker with the frame length of d=200 and an oscillation angle of* $\psi_0 = 120°$

The individual lengths of the links can be determined on the basis of the dead-center construction according to Alt [16], but a dynamic investigation is still required to find the proper constellation.
Figure 5 shows the right part of the crank rocker that has been cut free, so that the coupler and rocker remain and the rod force F_K in the coupler could be determined, see equation 4.

$$F_K = \frac{-\ddot{\gamma}(I_{S3} + r_3^2 m_3) - M_{ab}}{c \sin(\mu)} \tag{4}$$

The determining term in equation 4 is the mass inertia force, which is mainly formed by the angular acceleration $\ddot{\gamma}$ of the rocker arm.

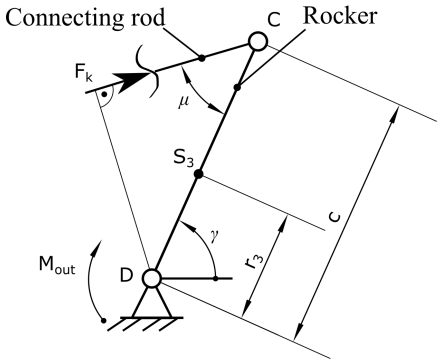

Figure 5. *Mathematical model of the crank rocker with cut free coupler*

Figure 6 shows the angular acceleration curve $\ddot{\gamma}$ for different solutions depending on β, which fulfill the condition of the centric crank rocker, over the drive coordinate q. Here the drive speed is constant at $\dot{q} = 20\frac{rad}{s}$ and the calculation of $\ddot{\gamma}$ is based on the equation 5.

$$\ddot{\gamma} = \frac{\mathrm{d}\dot{\gamma}}{\mathrm{d}t} = \gamma'' \cdot \dot{q}^2 + \gamma' \cdot \ddot{q} \tag{5}$$

It can be seen that the smaller β, the lower the angular acceleration and consequently the rod force F_K decreases.
To determine all constraining forces in the joint nodes, a mechanical equivalent model of the crank rocker is created. The equation of motion of the system is defined and with the known course of the drive angular velocity the joint forces are determined.

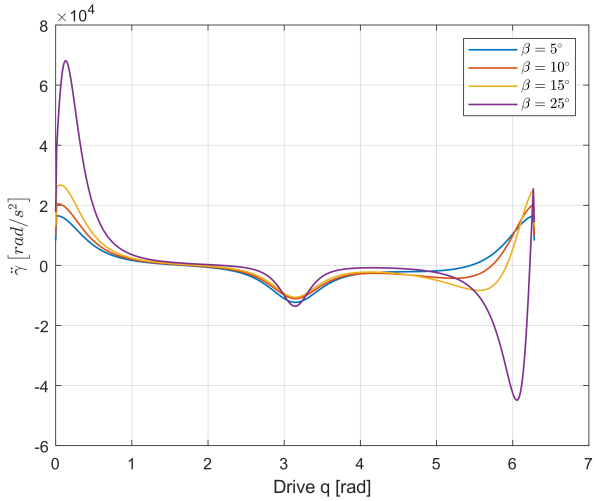

Figure 6. *Angular acceleration* $\ddot{\gamma}$ *over the drive coordinate, for different solutions depending on* β

Presented at 47th European Rotorcraft Forum, United Kingdom, 7-9th September, 2021

2.1.4 Design

The essential requirement for the freewheel gearbox in the compound split is to achieve a transmission ratio of $-\infty \leq i \leq 0$. To reach this transmission range, the combination of two freewheel gearboxes is necessary, which are connected via the central-gear. Since the direction of rotation of the input and output shafts of the freewheel gearbox is the same, an additional reversing gearbox is required so that the transmission ratio becomes negative. The functional diagram of this design with the combined freewheel gearboxes is shown in Figure 7, where system A takes over the transmission range of $-\infty \leq i \leq -1$ and system B is required for $-1 \leq i \leq 0$. At system A, drive is done by cranks (A1), which set crank rocker in motion and so planet wheels (A2) drive the central wheel (A3). At system (B) now the central wheel (B3) drives the planet wheel (B2), so the crank rocker mechanism (B1) is the output.

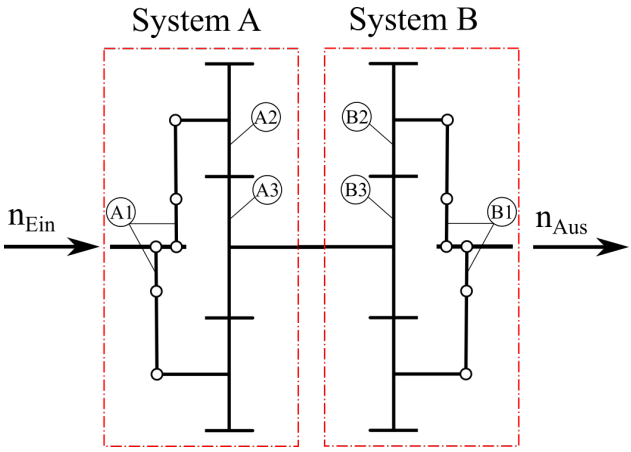

Figure 7. *Functional schematic of two combined freewheel gearboxes*

2.1.5 Mass estimation

The boundary conditions of the compound split result in a high drive torque. To reduce the high input torque, a planetary gear is connected before and after the freewheel gearbox, see Figure 8. The first planetary gear is driven via the carrier (s) and the output is driven via the sun gear (1) to the variator. In contrast, in the second planetary gear the input is driven via the sun gear and the output via the carrier. As both planetary gearboxes have the same fixed carrier ratio, a speed change is only made in the variator train. The mass estimation of a planetary gear follows from the work of H. Amri [18] where the carrier ratio and the torque at the sun gear are needed.
As a result, the input speed to the variator is transformed into high speed at constant power and back into low speed after the variator, which reduces the

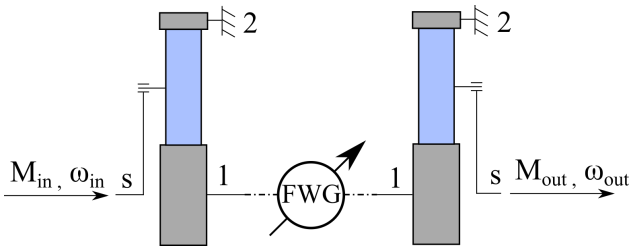

Figure 8. *Variator train with freewheel gearbox (FWG) and up- and downshifted planetary gears*

torque in the freewheel gearbox. This in turn has a positive effect on the tooth root and tooth flank stresses therefore, the center distance as well as the mass of the spur gears can be reduced.
For the mass estimation, a spur gear pair from the freewheel gearbox, which consists of a central gear and a planetary gear, is taken out and subjected to a strength analysis using the KISSsoft calculation software. With the help of the KISSSoft fine sizing tool, a large number of solutions are generated which meet the boundary conditions. The solutions which represent a mass minimum are used for the mass estimation. The calculation of the spur gears is performed for the critical transmission range where a high drive torque and simultaneously low speed is dominant.

2.2 Results for the Freewheel IVT

To keep the speed fluctuation as low as possible the determining factor is how many planet wheels can be arranged around the central wheel. The more the better, but this has a negative effect on the total mass. For the required case with a spur gear ratio of $i_{St} = 0.8$, a maximum of five planet wheels can be fitted. Depending on the crank length, which serves to vary the transmission ratio, the speed fluctuation varies and has a non-linear course. The maximum fluctuation is about 8%. The input speed has no influence on the speed fluctuation at the drive output.
To keep the joint forces in the crank rocker low, the centric crank rocker is used. From the dynamic analysis of the centric crank rocker, it can be concluded that the ideal solution is where the angle β is small. This follows from the fact that the angular acceleration $\ddot{\gamma}$ of the rocker arm is thereby reduced and consequently the inertial forces decrease. For further analysis, a centric crank rocker with an angle of $\beta = 10°$ and the corresponding link lengths are used.
For the mass estimation it follows that if no planetary gearbox is shifted before and after the freewheel gearbox, the mass of the spur gears is 271 kg. This is mainly due to the high driving torque. If, on the other hand, a planetary gearbox is placed before and after it, the mass of the spur gears and both planetary gearboxes results in a mass of 131 kg. The housing,

Presented at 47th European Rotorcraft Forum, United Kingdom, 7-9th September, 2021

freewheels, bearings and crank rockers are not taken into account in the mass estimation.
With the coupling of two freewheel gearboxes, its complexity with regard to dynamic behaviour increases. In order to determine the properties of the system in more detail, the multibody simulation (MBS) software Simpack is used. It turned out that system B does not fulfill the desired motion. The reason is the kinematic condition of the system, which causes the freewheel to open or block permanently. This gained knowledge also corresponds to the result of C. Pelger [14].
Figure 9 shows a section of a spur gear pair in which the central wheel drives the planet wheel and between the planet wheel and the rocker arm there is a frictionally engaged freewheel with a sprag element, as shown in Figure 10 and 11. This drive mode corresponds to the system B from Figure 7, whereby the transmission ratio of $-1 \leq i \leq 0$ should be realized.

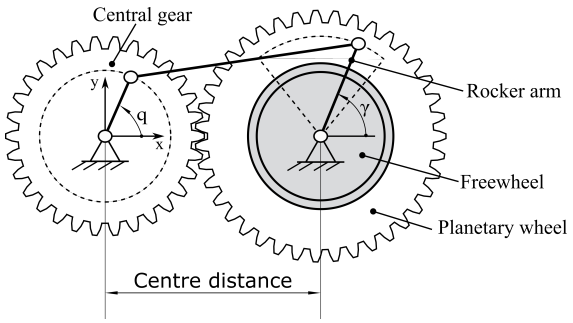

Figure 9. *Section of a spur gear pair and the corresponding crank rocker, based on C. Pelger [14]*

The outer ring of the freewheel is driven by the planet wheel and the inner ring would now be the output to the rocker arm. Since the planet wheels are in contact with the central wheel, all outer rings of the freewheel have the same angular speed and direction of rotation. If now the planet wheel turns counter-clockwise and the outer ring is in locking direction and the system is raised from standstill, all rockers have the same direction of rotation. In order for the cranks to rotate in one direction, the rockers must have a nonlinear angular path. This is not possible and the system is blocked.

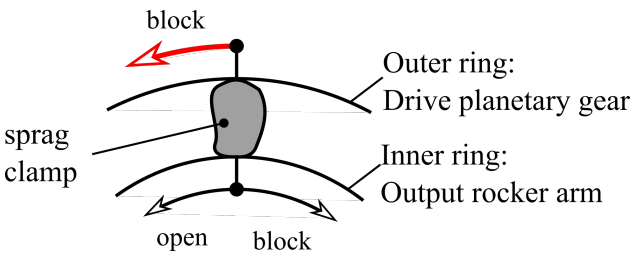

Figure 10. *Orientation of the freewheeling and locking direction of the outer and inner ring of a sprag freewheel [19]*

If the freewheel direction is now reversed so that the outer ring of the freewheel is in freewheel-mode in an anti-clockwise direction, then no rocker arm can be driven and the system remains at rest.

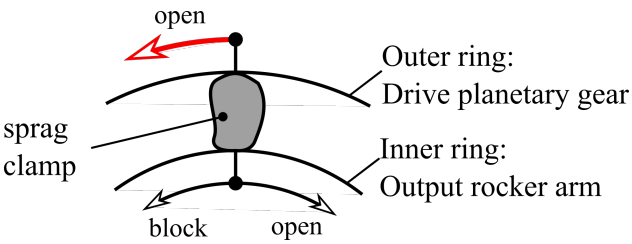

Figure 11. *Orientation of the freewheeling and locking direction of the outer and inner ring of a sprag freewheel [19]*

Due to these conditions, the freewheel blocks the movements of the rocker arm or it is permanently open and no force is transmitted. Therefore, system B does not meet the requirements and the achievable transmission ratio of the system is $-\infty \leq i \leq -1$.

3 THE TRACTION IVT

3.1 Traction-IVT Model

3.1.1 Geometric Relationships

The traction drive presented in this chapter is based on the CVP (continuously variable planetary) traction drive described in References [20] & [21], which is mainly used as a continuously variable transmission for electric bycicles. It consists of five main components, depicted in Figure 12: The hollow shafts A and B, the sun shaft C and the carrier shaft D as well as traction elements. Shafts A, B and C contact the traction spheres under heavy pressure of several GPa, which allows the traction fluid inside the contact patches to exhibit a considerable traction coefficient in order to transmit torque. The transmission ratio can be continuously varied by manipulating the angle γ between the rotational axis of the traction sphere and the coaxial shafts. This leads to a change of the radii R_{AB}, R_{BB} and R_{CB} between the contact patches and the spheres axis of rotation. The influence of the variation of these radii corresponds to manipulation of the radii of the planet gears in the kinematic planetary analogy given in Figure 12 from Ref. [21].

3.1.2 Kinematic Model

The different shafts have been separated in order to describe the kinematic relationships. Sections of the traction sphere which are normal to its rotational axis have been created and depicted in Figure 13. The

Presented at 47th European Rotorcraft Forum, United Kingdom, 7-9th September, 2021

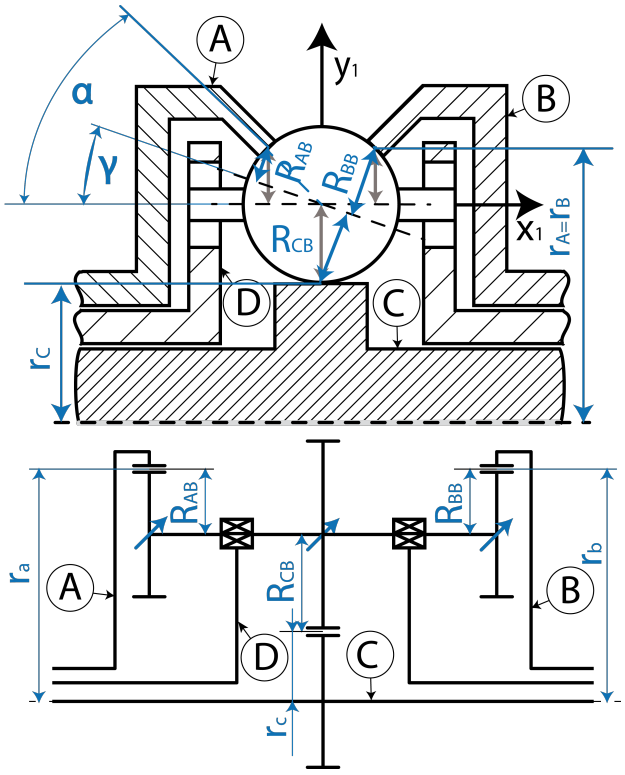

Figure 12. *Schematic of the traction drive CVT and kinematic analogy from Ref. [21]*

relationship between the rotational velocities of the shafts $\omega_{A,B,C}$ and the velocities of the contact points $v_{BA,BB,BC}$ is described by the corresponding radius $r_{A,B,C}$ and the value of creep $C_{RA,RB,RC}$ in Equation 6. The exponent is positive for input shafts and negative for output shafts.

$$(6)\quad v_{BA,BB,BC} = r_{A,B,C} * \omega_{A,B,C} * (1 - C_{RA,RB,RC})^{\pm 1}$$

Additionally, the velocity of the traction spheres axis $v_{DA,DB,DC}$ at the center of every section $S_{A,B,C}$ is given with the center distance $H_{IA,IB,IC}$ in Equation 7 and 8. Calculations for shaft A and B receive negative sign, while those for shaft C receive positive sign.

$$(7)\quad H_{IA,IB,IC} = r_{A,B,C} \pm R_{AB,BB,CB} * cos(\gamma)$$

$$(8)\quad v_{DA,DB,DC} = \omega_D * H_{IA,IB,IC} = v_{BA,BB,BC} \pm \omega_K * R_{AB,BB,CB}$$

As the rotational velocities of two shafts are set, Equation 6 to 8 allow for computation of the velocities of every element and shaft under assumption of creep.

3.1.3 Traction Model

A traction model has been set up in order to determine the traction drives' force-transmission-capabilities. In this traction model pressure, viscosity and velocity distribution are evaluated for every discrete point inside the contact. Film thickness is calculated as a base for a traction model. This traction model ultimately yields a maximum traction coefficient μ_{max} for every occuring transmission ratio. At first, the pressure distribution inside the contact is calculated according to hertzian theory. Although the contact patch for NuVinci type traction drives is generally elliptic, a circular contact is assumed. The hertzian formulae for contact size and pressure distribution in the circular or axisymmetric problem are taken from [22]. After pressure has been evaluated, the relationship between pressure, temperature and viscosity is described, using the improved Yasutomi free volume model from Ref. [23] with data from Ref. [24] for the traction fluid Santotrac 50. The Hamrock & Dowson newtonian film thickness calculations for circular contacts are used, as described in [25]. Since the traction fluid Santotrac 50 is known to exhibit shear thinning behaviour at higher rolling speeds, which reduces viscosity and film thickness, this non-newtonian effect has to be considered [26], [27]. This is accomplished by including a film-thickness reduction factor from [28] with data for Santotrac 50 by [28] and [29]. The impact of shear thinning on viscosity itself is neglected since this effect becomes negligible for traction at high pressures [30]. In order to calculate traction, two traction models are used: The Bair & Winer traction model under viscoplastic assumption [31] as seen in [32] and the Johnson & Tevaarwerk Model for maximum shear stress [33].

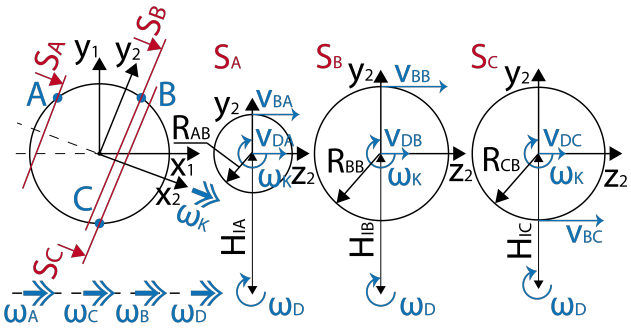

Figure 13. *Geometric relationships of the velocities for the traction drive*

3.1.4 Force Model

A similar approach to the kinematic model is used for the force model: The shafts are separated from each other and the forces relevant to the power transmission of the traction drive are displayed in Figure 14. Utilizing a stationary approach, the torque equilibrium for shafts A, B and C is given in Equation 9 with

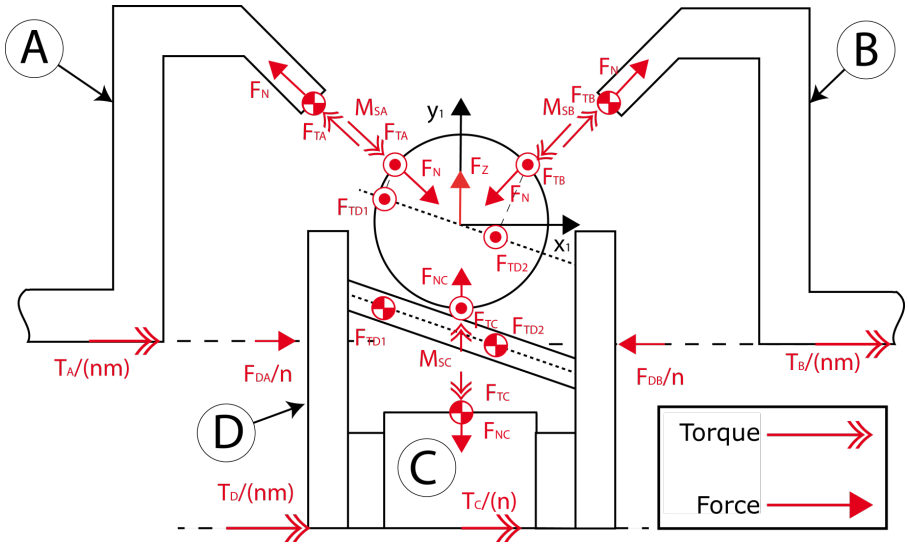

Figure 14. *Force-Model for the traction drive*

the number of rows of traction spheres m, the number of traction spheres per row n and traction forces $F_{TA,TB,TC}$.

$$T_{A,B,C} = F_{TA,TB,TC} * r_{A,B,C} * m * n \tag{9}$$

Similarly, the torque equilibrium for shaft D is given in Equation 10 with the forces F_{TD1} and F_{TD2}, which are acting upon the traction spheres axis in the previous sections S_A and S_B.

$$T_D = (H_{IA} * F_{TD1} + H_{IB} * F_{TD2}) * m * n \tag{10}$$

Additionally, the force and torque equilibrium for the traction sphere is given in Equation 11 and 12.

$$0 = F_{TA} + F_{TB} + F_{TC} + F_{TD1} + F_{TD2} \tag{11}$$

$$0 = F_{TA} * R_{AB} + F_{TB} * R_{BB} - F_{TC} * R_{CB} \tag{12}$$

Although spin is accounted for in the calculation of traction, spin related torques $M_{SA,SB,SC}$ as seen in Figure 14 are neglected under the assumption that $M_{SA,SB,SC} \ll T_{A,B,C}$.

Furthermore, a relationship between force in the axial direction of the shafts A and B $F_{DA,DB}$ and the normal force on the traction contact F_N as well as F_{NC}, which is necessary to transmit force, is given in Equation 13 and 14.

$$F_N = F_{DA,DB} \frac{cos(\alpha)}{n} \tag{13}$$

$$F_{NC} = 2F_N sin(\alpha) - F_Z \tag{14}$$

F_Z being the radial force due to inertia, which is calculated in Equation 15.

$$F_Z = m_K(R + r_C)\omega_D^2 \tag{15}$$

3.1.5 Design

A design model was set up for an automatic mass calculation driven by the optimization of the main design parameters. The assignment of the design criteria to the different components is shown in Figure 15: The numbers (1) to (6) correspond to the critical design factor for sizing of each component (e.g. bending and torsional stresses in shafts or fatigue life of traction contacts). The shafts are dimensioned using preliminary design relationships due to material, diameters and torsional (1), as well as bending (2) stresses taken from [34][S. 297]. The hollow shafts A and B are additionally sized due to radial bending (5) stemming from the equally spaced contact forces between shaft and every traction spheres F_N as given in [35]. Additionally, these hollow shafts have a disk attached to them at their outermost end, which serves as a base for a roller bearing, used to achieve the axial forces required for providing the contact pressure in the traction contact. This disk-like geometry is also subject to severe bending stresses (6) and sizing is accomplished by using the Bernoulli-Euler and the Kirchhoff disk theorem as presented in [36][S.299ff], which allows for calculation of occuring stresses and deformation of circular disk elements. The planet carrier, which is connected to shaft D, is modeled as a slotted disk. The slots allow for tilting of the traction sphere axles, necessary to manipulate the transmission ratio. The minimum distance of the slotted holes from each other and the border of the disk as well as the thickness of the disk due to bolt-bearing stress (4) is calculated using the Eurocode 3, which is usually meant for the calculation of bolted joints, as a rough estimate. Finally, the length of life (3) is evaluated for all bearings according to DIN 281 and for every traction contact using the lifecycle model for traction contacts presented in [37]. After the gen-

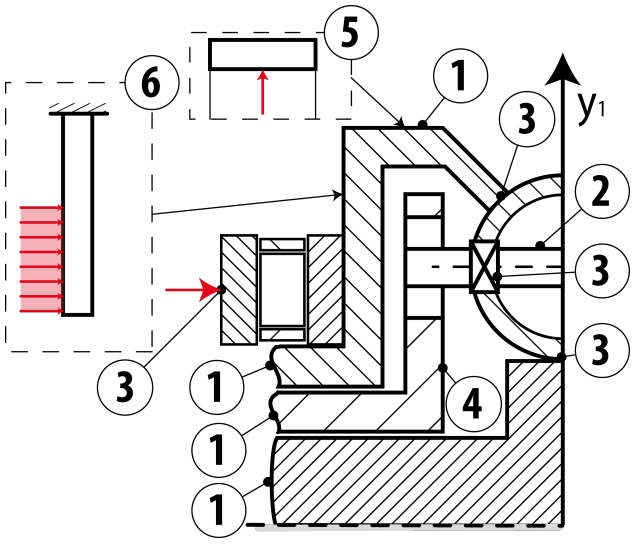

Figure 15. *Assignment of dimensioning criteria*

eral part dimensions have been evaluated, component mass can be calculated or - in terms of the bearings - automatically picked from the catalogue data. Additionally, the mass of possible planetary stages and spur gears, which are used before as well as after the traction drive in order to reduce torque inside the drive or to collect the torques from multiple parallel traction drive stages is estimated using the relationship between mass, torque and transmission ratio given in Ref. [38].

3.1.6 Optimization

The design model presented in subsubsection 3.1.5 is utilized to automatically generate and size every described shaft, bearing and planet carrier, as long as input torques and velocities as well as material and the principal geometric values that govern the kinematics of the traction drive (α & γ) are given. The requirement of setting the principal geometric values allows for determination of the kinematic properties of the traction drive while other dimensions can be chosen in order to minimize mass. Three independent values have been found for optimization: the outer radius of shaft C r_C, the number of parallel traction drive stages or cavities m and the transmission ratio of possible planetary stages before and after the traction drive i_{PG}. In order to conduct any optimization, the definition of an objective goal is required. These goals need to be quantified and weighted and finally merged into a single value - the *fitness* - to be used in an genetic algorithm optimization process. Two types of goals were defined:

Primary goals:

- Transmit required maximum torque
- Maintain component life above minimum
- Maintain film thickness above minimum
- Avoid collisions

Secondary goals:

- Minimize mass

Primary goals are either quantified by their negative relative distance to their upper or lower boundary value or equal to zero, if they are leading to an acceptable solution. It is necessary to provide the optimization algorithm with the information about *how much off* an unusable configuration is. Only when the sum fitness of all primary goals reaches zero, the secondary goal is quantified, which leads to a description of the mass of the certain configuration relative to a reference mass (in this case 126kg). The sum of the fitness related to every subgoal is finally maximised, leading to a working configuration with minimum mass within this model. The flow chart in Figure 16 shows the general sequence of calculation, which is applied in the subsections above.

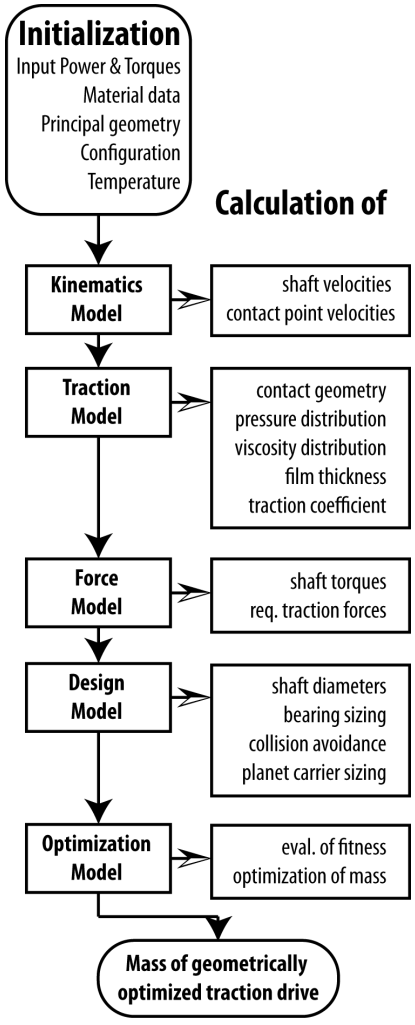

Figure 16. *Flow chart of the traction CVT evaluation and optimization model*

Presented at 47th European Rotorcraft Forum, United Kingdom, 7-9th September, 2021

3.2 Results for the Traction IVT

In order to accomplish the desired transmission ratio range of $-\infty \leq i_V \leq 0$ different configurations of the described traction drive have been evaluated and two design strategies have been found in order to create infinite or zero-transmission. Infinite or zero transmission corresponds to a state in which the input- and output-shafts are decoupled. The first strategy was to find an assignment of shafts, for which these boundary transmission values can be reached, simply by tilting the traction sphere without additional components. Since this relies on one shaft standing still, while the other exhibits rolling without torque transfer, there exists the problem of traction and film thickness as rolling velocities of one contact slowly reach zero. Both the Johnson & Tevaarwerk traction model as well as the Hamrock & Dowson model for film thickness require nonzero rolling speed. The isothermal viscoplastic Bair & Winer Model can be used for traction calculations with creep of less than 10% - but zero rolling speed results in infinite creep. The first strategy can not be modeled using the described methods. The second strategy thus requires the shafts of the traction drive never to stand still, while the shafts of the compound split are allowed to have zero velocity one at a time. This is achieved with one planetary differential stage on each end of the traction drive. The sun gears of both differential stages is connected to the central shaft C, while the ring gear of each stage is connected to either the shaft A on the input or the shaft B on the ouput side. Lastly, the planet carrier is connected to the input or output shaft. This results in the described kinematic phenomenon, when the axis of the traction sphere is tilted such that the speed ratio of shaft C and shaft A or shaft C and shaft B corresponds to the base transmission i_{21} of the connected differential stages. This setup is displayed in Figure 19.

3.2.1 Mass

Figure 17 shows the resulting mass of the design model for parameter variation of the unscaled transmission ratio of a planetary stage at the input and the output of the variator module i_{PGu} and the outer radius of shaft C r_C, while the number of ball rows is held constant at $m = 6$. i_{PGu} ranges from 0 to 1 and corresponds to the actual transmission ratio of the planetary stages as follows:

- $i_{PG} = i_{PGu}$ for $i_{PGu} < 0.42$
- $i_{PG} = 1$ for $0.42 < i_{PGu} < 0.6$
- $i_{PG} = 4 * i_{PGu}$ for $0.6 < i_{PGu} < 1$

This scaling between i_{PG} and i_{PGu} is necessary since the utilized genetic optimization algorithm does not allow for dicontinuities in the optimization parameters which in this case obviously happen due to the usual transmission ranges for planetary gears.

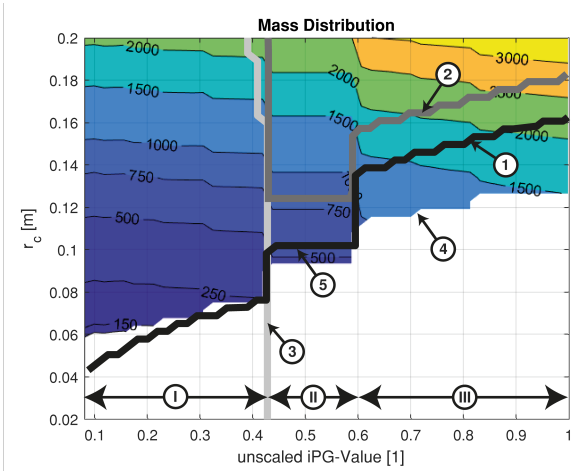

Figure 17. *Results of parameter variation of i_{PGu} and r_C at $m = 6$*

The scaling of these parameters leads to the three zones in Figure 17: Zone I denotes transmission to higher speeds, zone II no transmission ratio and zone II transmission to lower speeds. In general, masses increase strongly with increasing r_C, due to the resulting radial scaling of the whole gearbox and increase moderately with rising transmission ratio i_{PG}. At the boundaries of every zone, a discontinuity of mass takes place because of the corresponding discontinuity in transmission ratio. When including the primary design goals in the resulting mass, three design criteria are most relevant to the mass distribution shown in Figure 17: All configurations below (1) do not allow for sufficient force transfer in the traction contact according to the viscoplastic Bair & Winer traction model. Similarly, every configuration outside of (2) cannot provide force transfer in the Johnson & Tevaarwerk Model. The vertical cutoff between zones I and II happens for (2) because of the model boundaries in terms of rolling velocity. The second relevant design criterion is shown by (3) and displays the boundary for the fatigue life of the hertzian contacts: Since pressure is held constant in the contact and rotational velocity increases in zone I compared to zone II, the hertzian contact cannot support enough load cycles to provide for the necessary component life of 5000 hours. Thus every configuration left to the fatigue life boundary is not valid. Lastly, the value-less area confined by (4) does not provide masses, because no geometrically fitting bearings could be found in the SKF-bearing catalogue. The mass minimum has been found by the genetic algorithm at $r_C = 0.1m$ and $0.42 < i_{PGu} < 0.6 \rightarrow i_{PG} = 1$ for the viscoplastic Bair & Winer Model. The result of the genetic algorithm corresponds exactly to the mass minimum found by

Presented at 47th European Rotorcraft Forum, United Kingdom, 7-9th September, 2021

parametric variation in Figure 17 at (5) with 585kg. The use of genetic optimization led to an approximate 50-fold reduction in computational time using an Intel ®Core© i7-3610QM CPU@2.30GHz.

3.2.2 Dimensions

Due to the utilization of $m = 6$ rows of traction elements, the outer diameter of the lightest valid configuration is equal to 0.52m, with an absolute length of 1m. Although the mass of the connection mechanism of the traction drives rows is included in the mass estimation model, its dimensions have not been evaluated.

3.2.3 Efficiency

In Figure 18 the power flow over the variator module is compared to the flow over the shafts in the traction drive. Figure 18 (1) shows the point of maximum power flow over the variator module at about 200kW. Due to the introduction of differential planetary stages, power recirculation over the shafts A, B and C takes place. The recirculating power exceeds the maximum transmitted power through the variator module by 560% at the transmission boundaries e.g. as seen in Figure 18 (2). This excessive amount of circulating power generally impacts efficiency negatively. Additionally, power which is converted into heat needs to be removed from the CVT since increasing temperatures lower the force transfer capabilities.

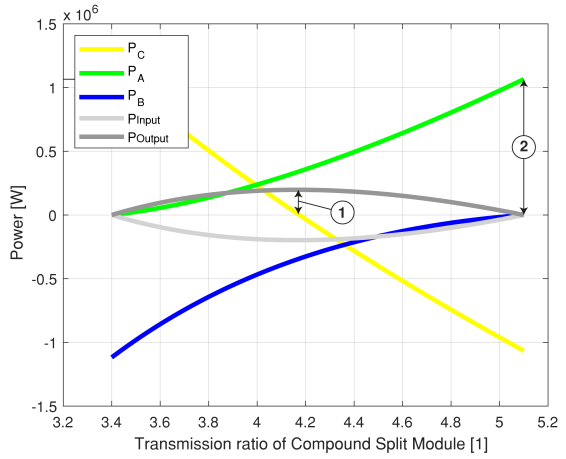

Figure 18. *Power flow of input and output shafts of the variator module compared to shafts of traction drive configuration*

4 DISCUSSION

Previous work conducted in [39] has calculated the maximum economic mass for a variable speed gearbox according to helicopter and mission type. Maritime search & rescue missions allow for the greatest additional weight with 445kg and are closely followed by external transport missions with 413kg. Both masses were calculated for the UH60A *Black Hawk*.

With regard to the mass reduction of the freewheel gearbox, a planetary gear is connected upstream and downstream in the variator train so that the input speed in the variator is increased and the torque to be transmitted decreases. Thereby, a mass minimum of $m = 131kg$ is achieved for the spur gears of the freewheel gearbox. The transmission range of $-\infty \leq i \leq 0$ can not be reached with the freewheel gearbox.

The traction IVT has the required transmission range of $-\infty \leq i \leq 0$. The presented traction drive concept has an outer diameter of 0.52m and a length of 1m. The great length is associated with the number of traction element rows $m = 6$. The outer diameter is only representative for the traction drive *without* the row-connection mechanism, which has not been evaluated in size. Thus, the dimensions roughly correspond to those of a UH-60A main gear box with an outer diameter and height of about 0.8m and 0.6m.

With 585kg solely for the variator module and excluding its housing, the presented traction drive concept already exceeds the overall maximum economic weight of 445kg. Yet it is necessary to point out, that the described model only leads to a *rough* estimation of mass and significant improvements are likely in the event of further and more detailed concept studies based on the automatically generated configuration.

Although the efficiency itself has not been evaluated, it is presumed to be significantly affected by the maximum recirculating power, which amounts to about 560% of the maximum transmitted power through the variator module. Since only about a maximum 10% of total main rotor power are diverted through the variator module, total efficiency is not very sensible on variator efficiency. Still, it is necessary to remove the generated heat from the variator assembly in order to maintain traction capabilities, which can lead to excessive requirements on cooling.

5 CONCLUSION

Two continuously variable transmission technologies have been evaluated for their use in variable speed drivetrain for rotorcraft using a compound split mechanism combined with a variator module. Both CVTs have been assessed in terms of capability of providing the necessary transmission ratio of $i = -\infty \rightarrow i = 0$ and the mass of their driving components excluding the housing.

- With the expectation of reduced mass in future conceptions of the presented traction drive, its

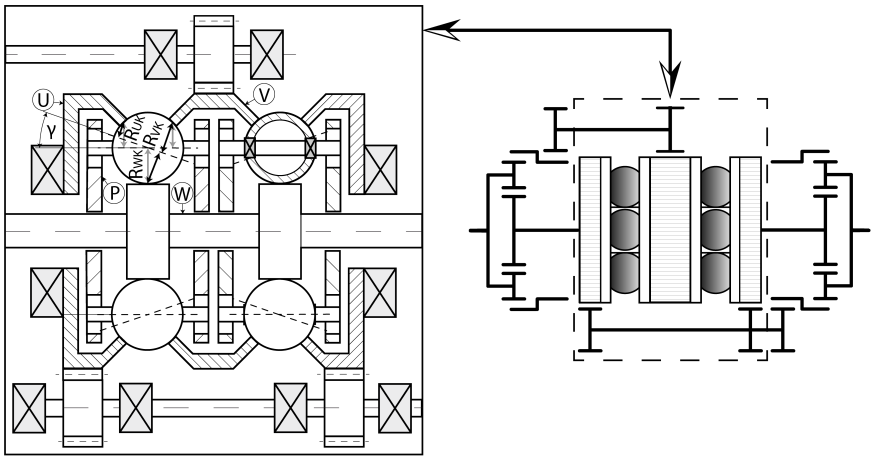

Figure 19. *Schematic of the chosen shaft configuration*

utilization in a UH-60A helicopter is generally plausible.

- The freewheel gearbox in the compound split is unsuitable for a helicopter, since the required transmission ratio is not achieved.
- The traction gearbox based on the NuVinci traction drive concept requires additional differential planetary stages in order to provide the necessary transmission ratio.
- The freewheel gearbox is only capable of a transmission ratio of $-\infty \leq i \leq -1$.
- Combination of a mirrored freewheel gearbox assembly in order to allow for the necessary transmission ratio has not been successful due to the nature of the freewheel mechanism.
- The mass of the lightest configuration found with the provided model amounts to 585kg for the shafts, bearings, traction elements, spur gears and planetary stages.
- With a mass of the spur gears of only 131kg, the freewheel gearbox provides a very light solution compared to the traction IVT.
- The differential planetary stages lead to high recirculating power, which is generally associated with low efficiency.

ACKNOWLEDGEMENT

The project VARI-SPEED is supported by the German Federal Ministry for Economic Affairs and Energy in the program LuFo and by the Austrian Federal Ministry for Transport, Innovation and Technology in the program Take Off. Partners are Vienna University of Technology (Austria), Munich University of Technology (Germany) and Zoerkler Gears GmbH (Austria). The authors would like to thank KISSsoft AG for the possibility to use their design software KISSsoft.

REFERENCES

[1] U.S. Army, "Future vertical lift (fvl) capability set 1 request for information."

[2] European Aeronautics Industry, "Clean sky 2 joint technical program."

[3] M. Hirschberg, "Clean sky 2 update, part 1: The airbus racer," *Vertiflite*, vol. 63, pp. 26–28, Sep./Oct. 2017.

[4] G. A. Misté, "Variable speed rotor helicopters: Optimization of main rotor - turbo shaft engine integration," 2015.

[5] W. Johnson, G. K. Yamauchi, and M. E. Watts, "NASA Heavy Lift Rotorcraft Systems Investigation," tech. report, NASA Ames Research Center and Langley Research Center, 2005.

[6] J. C. W. Acree, H. Yeo, and J. D. Sinsay, "Performace Optimization of the NASA Large Civil Tiltorotr," tech. report, NASA Ames Research Center, Moffett Field, California 94035, USA, 2008.

[7] M. A. Stevens, R. F. Handschuh, and D. G. Lewicki, "Concepts for Variable/Multi-Speed Rotorcraft Drive System," Technical Memorandum 2008-215276, NASA, 2008.

[8] H. Amri, R. Feil, M. Hajek, and M. Weigand, "Possibilities and difficulties for rotorcraft using variable transmission drive trains," *CEAS Aronautical Journal*, vol. 7, pp. 335–346, June 2016.

Presented at 47th European Rotorcraft Forum, United Kingdom, 7-9th September, 2021

[9] W. Garre, T. Pflumm, and M. Hajek, "Enhanced efficiency and flight envelope by variable main rotor speed for different helicopter configurations," in *42nd European Rotorcraft Forum 2016*, 2016.

[10] W. Garre, H. Amri, P. Paschinger, M. Mileti, M. Hajek, and M. Weigand, "Helicopter configurations and drive train concepts for helicopter configurations and drive train concepts for optimal variable rotor-speed utilization," in *Deutscher Luft- und Raumfahtrkongress 2016*, 2016.

[11] H. Amri, K. Hartenthaler, and M. Weigand, "Mass and kinematic analysis of compound split with simulation of the shifting process for variable rotor speed," in *74th American Helicopter Scoiety Forum 2018*, 2018.

[12] H. Amri, F. Donner, L. Braumann, F. Huber, and M. Weigand, "Comparison of variator technologies for variable rotor speed drivetrains for rotorcraft," in *Proceedings of the 76th Annual Forum*, (Virtual), The Vertical Flight Society, October 2020.

[13] X. Su, H. DeSmidt, E. C. Smith, and R. C. Bill, "Modeling and design of a wet clutch offset compound gear transmission for dual-speed rotorcraft applications," in *Proceedings of the 76th Annual Forum*, (Virtual), The Vertical Flight Society, October 2020.

[14] C. Pelger, G. Jacobs, and F. Straßburger, *Das mechanische IVT: Idee / Funktion / Umsetzung.* Antriebstechnisches Kolloquium ATK: 107-122, 2015.

[15] O. Friedmann, W. Haas, and U. Mair, *Das Kurbel-CVT; Wirtschaftlicher als ein Handschaltgetriebe und komfortabler als ein heutiges CVT?* 07. LuK Kolloquium: 107-116, 2002.

[16] A. Fricke, D. Günzel, and T. Schaeffer, *Bewegungstechnik; Konzipieren und Auslegen von mechanischen Getrieben.* Hanser Verlag, 2019.

[17] VDI, *VDI-Richtlinie 2130: Getriebe- für Hub- und Schwingbewegungen: Konstruktion und Berechnung viergliedriger ebener Gelenkgetriebe für gegebene Totlagen.* Beuth-Verlag, Berlin, überprüft und bestätigt (2016), 1984.

[18] H. Amri, K. Hartenthaler, and M. Weigand, "Mass and kinematic analysis of compound split with simulation of the shifting process for variable rotor speed," *74th American Helicopter Society Forum 2018*, 2018.

[19] *Ringspann. Produktkatalog Freiläufe. https://www.ringspann.at/de/files/P84-D-140401-237.pdf [Online, viewed 10.04.2019].*

[20] R. Whisler, C. Schneider, M. Stone, and J. Carter, "An analytical approach for assessing cvt alternatives," in *Proc. of the 8th CTI Symposium*, (Rochester, MI), 2014.

[21] B. Pohl, M. Simister, R. Smithson, and D. Miller, "Configuration analysis of a spherical traction drive cvt/ivt," tech. rep., SAE Technical Paper, 2004.

[22] J. R. Barber, *Contact mechanics*, vol. 250. Springer, 2018.

[23] S. Bair, C. Mary, N. Bouscharain, and P. Vergne, "An improved yasutomi correlation for viscosity at high pressure," *Proceedings of the Institution of Mechanical Engineers, Part J: Journal of Engineering Tribology*, vol. 227, no. 9, pp. 1056–1060, 2013.

[24] P. Vergne and S. Bair, "Classical ehl versus quantitative ehl: a perspective part iâ€"real viscosity-pressure dependence and the viscosity-pressure coefficient for predicting film thickness," *Tribology Letters*, vol. 54, no. 1, pp. 1–12, 2014.

[25] B. J. Hamrock, S. R. Schmid, and B. O. Jacobson, *Fundamentals of fluid film lubrication.* CRC press, 2004.

[26] S. Blair, *High Pressure Rheology for Quantitative Elastohydrodynamics*, vol. 54. Elseveir, 2007.

[27] B. Villechaise, G. Dalmaz, J. Makala, and J.-P. Chaomleffel, "On the traction fluid behaviour in concentrated contacts," in *Tribology Series*, vol. 40, pp. 401–412, Elsevier, 2002.

[28] W. Habchi, S. Bair, F. Qureshi, and M. Covitch, "A film thickness correction formula for double-newtonian shear-thinning in rolling ehl circular contacts," *Tribology Letters*, vol. 50, no. 1, pp. 59–66, 2013.

[29] S. Bair, "The rheological assumptions of classical ehl: what went wrong?," *Tribology International*, vol. 131, pp. 45–50, 2019.

[30] Y. Liu, Q. J. Wang, S. Bair, and P. Vergne, "A quantitative solution for the full shear-thinning ehl point contact problem including traction," *Tribology Letters*, vol. 28, no. 2, pp. 171–181, 2007.

[31] S. Bair and W. O. Winer, "A rheological model for elastohydrodynamic contacts based on primary laboratory data," *Journal of Lubrication Technology*, vol. 101, no. 3, pp. 258–264, 1979.

[32] G. Carbone, L. Mangialardi, and G. Mantriota, "A comparison of the performances of full and half toroidal traction drives," *Mechanism and Machine Theory*, vol. 39, no. 9, pp. 921–942, 2004.

Presented at 47th European Rotorcraft Forum, United Kingdom, 7-9th September, 2021

[33] J. L. Tevaarwerk and K. Johnson, "The influence of fluid rheology on the performance of traction drives," *Journal of Lubrication Technology*, vol. 101, no. 3, pp. 266–273, 1979.

[34] H. Haberhauer and F. Bodenstein, *Maschinenelemente: Gestaltung, berechnung, anwendung*. Springer-Verlag, 2013.

[35] G. Németh, "Elementary calculations for deflection of circular rings," in *Vehicle and Automotive Engineering*, pp. 115–122, Springer, 2017.

[36] H. A. Mang and G. Hofstetter, *Festigkeitslehre*. Springer, 2018.

[37] S. H. Loewenthal and E. V. Zaretsky, "Design of traction drives," 1985.

[38] H. Amri, K. Hartenthaler, and M. Weigand, "Mass and kinematic analysis of a compound split with simulation of the shifting process for variable rotor speed," in *74th Annual American Helicopter Society International Forum and Technology Display 2018 (FORUM 74): The Future of Vertical Flight*, p. 8, American Helicopter Society, 2018.

[39] W. Garre, T. Amri, H. Pflumm, P. Paschinger, M. Mileti, M. Hajek, and M. Weigand, "Helicopter configurations and drive train concepts for optimal variable rotor-speed utilization," 2016.

Presented at 47th European Rotorcraft Forum, United Kingdom, 7-9th September, 2021